1. THE 2D HYDROTHERMAL FLOW MODEL

1.1 GOVERNING EQUATIONS

We assume the convecting fluid to be pure water flowing through a rigid porous medium. We will use indices f and r to refer to fluid and rock properties, respectively. Mass transport is described by Darcy's law

$$\vec{v} = -\frac{k}{\mu_f}\left(\nabla p - \rho_f \vec{g}\right) \tag{1}$$

where $\vec{v}$ the Darcy velocity, *k* is permeability, μ_f the fluid's dynamic viscosity, ρ_f fluid density, p pressure, and $\vec{g}$ the gravitational acceleration vector.

Fluid mass conservation is expressed by

$$\phi \frac{\partial \rho_f}{\partial t} = -\nabla \cdot \left(\vec{v}\rho_f\right) \tag{2}$$

with ϕ being the porosity of the rock. Substituting equation (1) into (2) and noting that the fluid's density is a function of temperature T and pressure yields the pressure equation

$$\phi\rho_f\left(\beta_f \frac{\partial p}{\partial t} - \alpha_f \frac{\partial T}{\partial t}\right) = \nabla \cdot \left(\rho_f \frac{k}{\mu_f}\left(\nabla p - \rho_f \vec{g}\right)\right) \tag{3}$$

where α_f and β_f are the fluid's thermal expansivity and compressibility, respectively.

Hydrostatic pressure at the Logatchev 1 hydrothermal field (~30 MPa) is above the critical endpoint of pure water (22.1 MPa) so that the fluid will always be in the single-phase region. This allows us to formulate energy conservation as a function of temperature:

$$\left(\phi\rho_f cp_f + (1-\phi)\rho_r cp_r\right)\frac{\partial T}{\partial t} = \nabla \cdot \left(K \nabla T\right) - \rho_f cp_f \vec{v} \cdot \nabla T + \frac{\mu_f}{k}\vec{v}^2 - \left(\frac{\partial \ln \rho}{\partial \ln T}\right)_p \frac{Dp}{Dt} \tag{4}$$

With cp being heat capacity and *K* the thermal conductivity of the rock. Fluid and rock are assumed to be in local thermal equilibrium (i.e. $T = T_r = T_f$) so that the mixture appears on the left-hand-side of equation (4). Changes in temperature depend on heat conduction (1st term on right-hand-side), heat advection by fluid flow (2nd term), heat generation by internal friction of the fluid (3rd term; viscous dissipation; e.g. (Magyari et al., 2005 p. 374)), and pressure-volume work including dependence of enthalpy on pressure (4th term, (Bird et al., 2007 p. 337)).

All fluid properties $(\alpha_f, \beta_f, \rho_f, \mu_f, cp_f)$ are functions of both pressure and temperature and are evaluated from pre-calculated look-up tables based on the IAPS-84 formulation of water and steam properties. The tables have been computed using the program PROST 4.1 (PROperties of water and STeam developed by Bauer (1998)), which is available at: http://fluidos.etsii.upm.es/faculty/Jaime_Carpio/Fumatas_negas/PROST%20Properties%20of%20Water%20and%20Steam.htm. The high water depth along the transect ensures that pure water remains at supercritical pressure-temperature (*P-T*) conditions so that two-phase phenomena do not need to be accounted for in our model.

1.2 NUMERICAL FORMULATION AND SOLUTION TECHNIQUES

We use 3-node triangular elements that form unstructured meshes of ~90e3 – 57e4 elements depending on the modeled fault width, which corresponds to elements sizes between 0.4 m^2 and 40 m^2 inside the fault/slot. We solve the equations for velocity (1), pressure (3), and temperature (4) separately. Using an implicit Finite Element Method (FEM) we solve equation (3) to derive the pressure field and subsequently (1) to obtain Darcy velocities. Equation (4) is solved by operator splitting: The advection term is treated by a semi-Lagrange scheme with 2nd-order accurate Predictor-Corrector integration along flow trajectories and a cubic interpolation scheme on the unstructured meshes. The diffusion part of the energy equation is also solved using an implicit FEM. This algorithm has been implemented into a modified version of the MATLAB code MILAMIN (Dabrowski et al., 2008). All matrix equations are solved using the Cholesky direct solver of the numerical library SuiteSparse (Davis and Hager, 2009) (http://www.cise.ufl.edu/research/sparse/SuiteSparse/).

1.3 BOUNDARY CONDITIONS

All domain boundaries are impermeable except the top boundary, through which the fluid is allowed to enter and leave the domain. All side boundaries are insulating. At the top boundary we use mixed boundary conditions: Temperature is set to 4˚C seawater temperature where fluid enters the domain, and at discharge nodes the vertical temperature gradient is set to zero $\left(\frac{\partial T}{\partial z} = 0\right)$ to mimic free venting conditions.

At the bottom boundary a Gaussian-shaped heat flux profile is applied

$$Hf(x) = Hf_{tot} \exp\left(-\frac{(x - x_0)^2}{2\sigma^2}\right), \quad (5)$$

where x_0 denotes the center of the heat source at x_0=6500m. Hf_{tot} is chosen such that the integrated heat-input along the transect is 12.5 kW per meter ridge axis — a reasonable value for the Mid-Atlantic Ridge (Sinha et al., 2004). The width of the heat source, controlled by

the half-width of the Gaussian curve, σ=1.25 km, was chosen based on the approximate lateral extent of the zone of enhanced seismicity in Figure 1. All calculations began with cold hydrostatic conditions and ran into thermal steady-state, at which all mass and energy fluxes balance and thermal energy inside the box remains constant.

2. ADDITIONAL RESULTS: ENHANCED BACKGROUND PERMEABILITY

We have conducted 32 additional runs with constant permeability contrast c = 10 between fault zone and surrounding but with enhanced background permeability ($1x10^{-15}$ m^2 and $2x10^{-15}$ m^2). The trend which is described in the main part of this paper is clearly also visible in these sets: Vent temperature decreases with increasing fault width (Fig. DR1a) while mass flux is increasing (Fig. DR1b). For any simulated fault width the vent temperature is decreased by ~40°C when the permeability of the background is doubled (Fig. DR1a), Consequently at the lowest background permeability ($5x10^{-16}$ m^2) the highest vent temperature is reached at the fault termination. The threshold width for deviation of the rising hydrothermal plume into the fault is decreased with increasing absolute background permeability (Fig. DR1.A). The fit between the grey lines and our data in Fig, DR1.B confirms that the modeled vent temperatures are can roughly be predicted by the theoretical solution described in the main text.

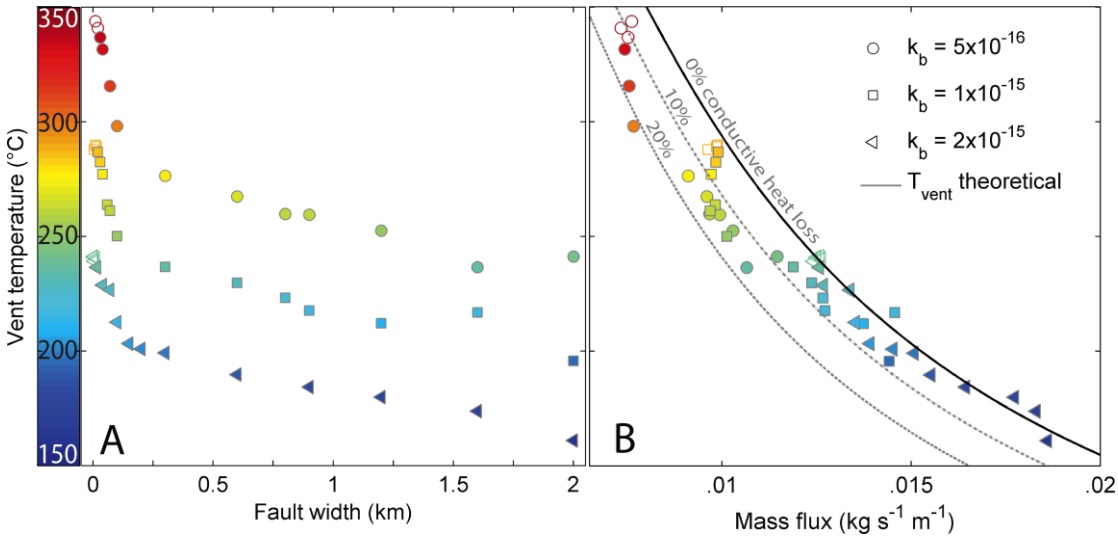

Figure DR1. Vent temperatures of additional simulations plotted against fault width and mass flux. The permeability contrast c = 10 is constant in all runs while the absolute background permeability k_b is changed. Symbols indicate different permeability contrasts, c, and their color shows maximum vent temperature. Filled symbols are simulations with venting at the fault tip at LHF1, open symbols indicate venting above the heat source. (A): Vent temperatures decrease with increasing fault width for each constant background permeability. The same is valid for any fault width and increased background permeability (B): Vent temperatures systematically decrease with increasing total mass flux through the seafloor. Model results are well fitted by theoretical vent temperatures calculated from the EOS for pure water (curves for 0, 10, and 20% conductive cooling at the seafloor) described in the main text.

REFERENCES CITED

Bauer, O., 1998, Prost 4.1 PROperties of water and STeam: TU Hamburg Harburg.

Bird, R. B., Stewart, W. E., and Lightfoot, E. N., 2007, Transport Phenomena, John Wiley & Sons.

Dabrowski, M., Krotkiewski, M., and Schmid, D. W., 2008, MILAMIN: MATLAB-based finite element method solver for large problems: Geochemistry Geophysics Geosystems, v. 9.

Davis, T. A., and Hager, W. W., 2009, Dynamic Supernodes in Sparse Cholesky Update/Downdate and Triangular Solves: Acm Transactions on Mathematical Software, v. 35, no. 4.

Magyari, E., Rees, D. A. S., and Keller, B., 2005, Effect of viscous dissipation on the flow in fluid saturated porous media, *in* Vafai, K., ed., Handbook of porous media: Boca Raton, Taylor & Francis Group, p. 374-406.

Sinha, M. C., Evans, R. L., German, C., Lin, J., and Parson, L., 2004, Mid-Ocean Ridges: Hydrothermal Interactions Between the Lithosphere and Oceans, p. 19-62.